Influence of Precursor on Microstructure and Phase Composition of Epitaxial Hydrothermal $PbZr_{0.7}Ti_{0.3}O_3$ Films

Magdalena Oledzka,[†] Malgorzata M. Lencka,[‡] Pascal Pinceloup,[†,||] Katherine Mikulka-Bolen,[†] Larry E. McCandlish,[§] and Richard E. Riman*,[†]

Department of Ceramic and Materials Engineering, Rutgers University, 607 Taylor Road, Piscataway, New Jersey 08854, OLI Systems, Inc., 108 American Road, Morris Plains, New Jersey 07950, and Ceramaré Corporation, 12D Jules Lane, New Brunswick, New Jersey 08901

Received January 31, 2002. Revised Manuscript Received August 13, 2002

Amorphous Zr−Ti hydrous oxide submicrometer spheres were employed in hydrothermal syntheses of $PbZr_{0.7}Ti_{0.3}O_3$ heteroepitaxial thin films on single-crystal $SrTiO_3$ substrates. Reactions utilizing processing variables that included precursor concentration (0.1−0.4 *m*), KOH concentration (6−12 *m*), and time (24−60 h) were carried out at 150 °C to evaluate the effect of this precursor on the formation of an epitaxial film. Selected experiments were also conducted to examine how this spherical precursor compares with two other precursor systems, that is, nanostructured amorphous Zr−Ti hydrous oxide prepared by coprecipitation at room temperature, and a mixture of crystalline TiO_2 and amorphous $ZrO_2 \cdot nH_2O$ obtained from soluble $ZrOCl_2 \cdot 8H_2O$. On the basis of the results of X-ray diffraction and electron microscopy, precursor choice, precursor concentration, and KOH mineralizer concentration have a significant effect on the quality, composition, and morphology of the film.

Introduction

Considerable research effort directed at synthesis and characterization of ferroelectric thin films has been driven in recent years by their potential applications in the manufacture of a variety of microelectronic devices.[1,2] These applications include integration of ferroelectric thin films for nonvolatile computer memories, transducers and actuators, infrared sensors, and electro-optic switches.[1] Single-crystal or epitaxial ferroelectric thin films are particularly interesting because materials with highly oriented structures may exhibit superior physical properties and arguably superior device characteristics, as compared to those of polycrystalline materials.[3,4]

Hydrothermal synthesis has been effectively applied to obtain thin films of lead titanate zirconate (PZT) and other perovskites.[5−10] Advantages of the hydrothermal method include simplicity (materials are synthesized directly from the solution, simple setup), low cost (relatively inexpensive precursors, lower processing temperature), and flexibility with respect to substrate shape and size.[11−13] Moreover, low processing temperature could mitigate interdiffusion and interfacial reactions that are detrimental to device properties.[14]

Application of hydrothermal epitaxy by various investigators has led to the syntheses of epitaxial films of perovskite and other oxide materials at temperatures 200 °C or below.[9,15−19] Chien et al.[9] demonstrated the epitaxial growth of $PbZr_{0.44}Ti_{0.56}O_3$ thin films on (001) $SrTiO_3$ and $LaAlO_3$ single-crystal templates at temperatures ranging from 90 to 150 °C and using anatase TiO_2, $ZrOCl_2 \cdot 8H_2O$ and $Pb(NO_3)_2$ as precursors and KOH as a mineralizer.

* To whom correspondence should be addressed. E-mail: riman@rci.rutgers.edu.
[†] Rutgers University.
[‡] OLI Systems, Inc.
[§] Ceramaré Corporation.
[||] Currently with KEMET, Greenville, SC.

(1) (a) Scott, J. F.; Paz De Araujo, C. A. *Science* **1989**, *246*, 1400. (b) Auciello, O.; Scott, J. F.; Ramesh, R. *Phys. Today* **1998**, *July*, 22−27.
(2) Haertling, G. H. *J. Am. Ceram. Soc.* **1999**, *82*, 797.
(3) Foster, C. M.; Bai, G.-R.; Csencsits, R.; Verone, J.; Jammy, R.; Wills, L. A.; Carr, E.; Amano, J. *J. Appl. Phys.* **1997**, *81*, 2349.
(4) Tuttle, B. A.; Voight, J. A.; Goodnow, D. C.; Lamppa, D. L.; Headley, T. J.; Eatough, M. O.; Zender, G.; Nasby, R. D.; Rodgers, S. M. *J. Am. Ceram. Soc.* **1993**, *76*, 1537.
(5) Kajiyoshi, K.; Ishizawa, N.; Yoshimura, M. *J. Am. Ceram. Soc.* **1991**, *74*, 369.
(6) Shimomura, K.; Tsurumi, T.; Ohba, Y.; Daimon, M. *Jpn. J. Appl. Phys.* **1991**, *30*, 2174.
(7) Ohba, Y.; Arita, K.; Tsurumi, T.; Daimon, M. *Jpn. J. Appl. Phys.* **1994**, *33*, 5305.
(8) Morita, T.; Kanda, T.; Yamagata, Y.; Kurosawa, M.; Higuchi, T. *Jpn. J. Appl. Phys.* **1997**, *36*, 2998.
(9) Chien, A. T.; Speck, J. S.; Lange, F. F. *J. Mater. Res.* **1997**, *12*, 1176.
(10) Su, B.; Ponton, C. B.; Button, T. W. *J. Eur. Ceram. Soc.* **2001**, *21*, 1539.
(11) Laudise, R. A. *Chem. Eng. News* **1987**, *28*, 30.
(12) Dawson, W. J. *Ceram. Bull.* **1988**, *67*, 1673.
(13) Kikuchi, T.; Tsurumi, T.; Ohba, Y.; Daimon, M. *Jpn. J. Appl. Phys.* **1992**, *31*, 3090.
(14) Lange, F. F. *Science* **1996**, *273*, 903.
(15) Chien, A. T.; Speck, J. S.; Lange, F. F.; Daykin, A.; Levi, C. *J. Mater. Res.* **1995**, *10*, 1784.
(16) Chien, A. T.; Zhao, L.; Colic, M.; Speck, J. S.; Lange, F. F. *J. Mater. Res.* **1998**, *13*, 649.
(17) Xu, W.-P.; Zheng, L.; Xin, H.; Lin, C.; Okuyama, M. *J. Mater. Res.* **1996**, *11*, 821.
(18) Chen, Q. W.; Qian, Y. T.; Chen, Z. Y.; Wu, W. B.; Chen, Z. W.; Zhou, G. E.; Zhang, Y. H. *Appl. Phys. Lett.* **1995**, *66*, 1608.
(19) Chen, Q. W.; Qian, Y. T.; Chen, Z. Y.; Zhang, Y. H. *Mater. Lett.* **1995**, *22*, 93.

10.1021/cm020063b CCC: $25.00
Published on Web 02/14/2003

In this work, we further explored the hydrothermal epitaxy of lead titanate zirconate by employing a new precursor, an amorphous Zr−Ti hydrous oxide composed of submicrometer spheres. We targeted films with the Zr-to-Ti ratio equal to 70:30, a composition that results in rhombohedral symmetry. [100]-oriented epitaxial PZT thin film with this symmetry might exhibit enhanced piezoelectric properties.[20] The main goal of our study was to examine the effect of the spherical Zr−Ti hydrous oxide precursor on the film uniformity and morphology under variable hydrothermal conditions. Also, we were interested in determining how the spherical precursor compares with the other precursors that have been previously employed in the hydrothermal synthesis of epitaxial PZT films, such as an amorphous nanostructured $Zr_{0.7}Ti_{0.3}O_2{\cdot}nH_2O$ oxide prepared by coprecipitation at room temperature[21] and a precursor composed of TiO_2 mixed with $ZrO_2{\cdot}nH_2O$ as precipitated from $ZrOCl_2$ solution by the addition of a KOH mineralizer.[9]

Experimental Section

1. Thermodynamic Modeling. A comprehensive thermodynamic model that simulates the behavior of heterogeneous systems containing a solid and an aqueous phase with dissolved electrolyte was successfully applied by Lencka et al. to rationally design the hydrothermal syntheses of a number of perovskite oxides, including lead zirconate titanate.[22,23]

We used this model as a tool for equilibrium calculations in the Pb−Zr−Ti−H_2O system. The details of the calculations have been presented elsewhere.[22] As a result of the calculations, the stability and yield diagram of the Pb−Zr−Ti−H_2O system at 150 °C has been computed (Figure 1). The diagram presents the optimum conditions for the synthesis of phase-pure $PbZr_{0.7}Ti_{0.3}O_3$. It guided the selection of various process conditions as well as facilitated interpretation of experimental results.

2. Materials. *Spherical Amorphous Precursor (SAP).* $Zr_{0.7}Ti_{0.3}O_2{\cdot}nH_2O$, hydrous spherical amorphous precursor oxide (referred to throughout the paper as the SAP oxide), was synthesized by thermal hydrolysis of a highly acidic 2-propanol−water solution containing zirconium(IV) propoxide, $Zr(OC_3H_7)_4$ (70 wt % in 1-propanol, Aldrich, Milwaukee, WI), and titanium(IV) isopropoxide $Ti(i\text{-}OC_3H_7)_4$ (97 wt % in 2-propanol, Aldrich). Choi et al. reported the synthetic method employed in this work.[24] However, metal alkoxides were used as sources of zirconium and titanium instead of inorganic salts such as $TiCl_4$ and $ZrOCl_2{\cdot}8H_2O$. Typically, the stoichiometric amounts of zirconium(IV) propoxide and titanium(IV) isopropoxide were dissolved in commercially available HCl aqueous solution (2 N, Fisher Scientific, Fairlawn, NJ) under vigorous stirring. 2-Propanol (Fisher Scientific), as well as hydroxypropyl cellulose, HPC (molecular weight ≈100,000 g/mol, Aldrich), which was a steric stabilizing dispersant for growth of unagglomerated particles, was subsequently added. The amount of HPC used was 0.3×10^{-3} g/mL of the final solution. The alcohol-to-water volume ratio and the total concentration of metal ions in this solution were 3.5 and 0.07 M, respectively. The solution was then homogenized by stirring for 6 h in a water/ice bath (≈4 °C). Finally, the container with the clear solution was transferred to a microwave (CEM Corporation, Matthews, NC), where the solution was uniformly heated to its boiling point without stirring. 4 M NH_4OH solution was added to the hot solution (to pH ∼ 10) to prevent the dissolution of the resultant coprecipitate upon cooling. The hydrous oxide was centrifuged with a Beckman induction drive centrifuge (Model J2-21M, Beckman Instruments, Palo Alto, CA) at 10 000 rpm for 5 min to remove alcohol. Later, the oxide was redispersed in deionized water (≈10 mΩ·cm; Milli-Q Water System, Millipore Corporation, Bedford, MA) with a Thermolyne Maxi Mix II, type 37600 mixer (Barnstead/Thermolyne, Dubuque, IA) and centrifuged again. Centrifugation and redispersion in water were done repeatedly until no chloride ions could be detected in a supernatant solution. Chloride ions were detected by the appearance of turbidity, which was accomplished by precipitating AgCl via the addition of $AgNO_3$ aqueous solution to the supernatant solution. The precursor was then used immediately for hydrothermal synthesis.

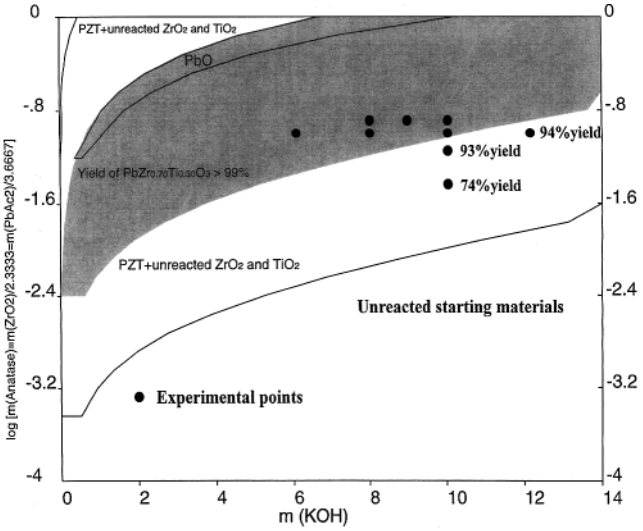

Figure 1. Stability and yield diagram in the Pb−Zr−Ti−H_2O system at 150 °C. Input Pb−Zr−Ti precursor concentration is plotted as a function of KOH concentration.

The composition of the precursor was analyzed semiquantitatively by standardless energy-dispersive spectroscopy (EDS) analysis. Precursor uniformity was assessed based on X-ray diffraction patterns recorded after its calcination at 1100 °C for 24 h. Particle size and shape were examined visually with a Leo-Zeiss Gemini 982 field emission scanning microscope (FESEM) (LEO Electron Microscopy, Inc., Thornwood, NY). The particle size was also measured in ethanol by dynamic light scattering (DLS) (DLS-700, Otsuka, Japan). Air-dried gel was further analyzed by thermogravimetric analysis (TGA) (TA Instruments, New Castle, DE) to determine the water content. TGA was performed in air (flow rate 5 mL/min) up to 1000 °C using a platinum pan with a heating rate of 10 °C/min. The specific surface area was measured by the multipoint BET method with N_2 as the adsorbate in a Coulter SA 3100 surface area analyzer (Coulter Corporation, Miami, FL). Prior to the measurement, the sample was vacuum-outgassed at ≈30 °C for 15 h. Crystallite size was estimated from the specific surface area data, assuming the powder had a density of 3 g/cm^3, was monodisperse, and had a spherical morphology.[25]

Nanostructured Amorphous Precursor (NAP). $Zr_{0.7}Ti_{0.3}O_2{\cdot}nH_2O$, hydrous nanostructured amorphous precursor oxide (later referred to as the NAP oxide), was prepared according to a known procedure (i.e., refs 21 and 22). Stoichiometric

(20) Du, X.-H.; Belegundu, U.; Uchino, K. *Jpn. J. Appl. Phys.* **1997**, *36*, 5580.

(21) Pinceloup, P.; Mikulka-Bolen, K.; Lencka, M. M.; McCandlish, L. E.; Burgener, P.; Riman, R. E. In *Perovskite Oxides for Electronics, Energy Conversion and Energy Efficient Applications*; Wong-Ng, W., Holesinger, T., Riley, G., Guo, T., Eds.; American Ceramic Society: Westerville, OH, 2000; Vol. 104 (*Ceramic Transactions*), p 253.

(22) Lencka, M. M.; Anderko, A.; Riman, R. E. *J. Am. Ceram. Soc.* **1995**, *78*, 2609.

(23) (a) Lencka, M. M.; Riman, R. E. *Chem. Mater.* **1993**, *5*, 61. (b) Lencka, M. M.; Riman, R. E. *J. Am. Ceram. Soc.* **1993**, *76*, 2649. (c) Lencka, M. M.; Nielsen, E.; Anderko, A.; Riman, R. E. *Chem. Mater.* **1997**, *9*, 1116. (d) Lencka, M. M.; Oledzka, M.; Riman, R. E. *Chem. Mater.* **2000**, *12*, 1323.

(24) Choi, J. Y.; Kim, C. H.; Kim, D. K. *J. Am. Ceram. Soc.* **1998**, *81*, 1353.

(25) Barringer, E. A.; Bowen, H. K. *Langmuir* **1985**, *1*, 414.

Table 1. Summary of Reactions[a] for the SAP Oxide, for the NAP Oxide, and for the CAP Oxide; Weight Gain, Film Type, 2θ Values of PZT (100) and (200) Peaks and Full-Width at Half-Maximum (FWHM) of the PZT (200) Peak of the Resulting Films

reaction no.	KOH (mol/kg of solvent)	$Zr_{0.7}Ti_{0.3}O_2$ (mol/kg of solvent)	time (h)	weight gain (mg)	film type	PZT (100) 2θ (deg)	PZT (200) 2θ (deg)	PZT (200) FWHM (deg)
				SAP Oxide				
40	6	0.3	48	0.81	opaque	21.492	43.718	> 10
52	8	0.3	48	0.58	semitransparent	21.589	43.912	4.7
57	9	0.4	60	0.39	transparent	21.593	43.960	4.0
31	10	0.1	24	0.02	transparent			
46	10	0.1	48	0.02	transparent			
42	10	0.2	48	0.50	transparent	21.976[b]	44.840[b]	0.7
30	10	0.3	24	0.07	slightly opaque	21.464	43.627	> 10
36	10	0.3	48	0.35	transparent	21.868	44.569	1.7
41	10	0.4	48	0.21	transparent	21.501	43.713	1.2
56	10	0.4	60	0.24	transparent	21.591	44.616	3.3
43	12	0.3	48	0.30	transparent	22.015[b]	44.893[b]	0.8
				NAP Oxide				
47	6	0.3	48	0.60	opaque	21.500	43.763	> 10
32	8	0.1	24	0.05	slightly opaque			
64	10	0.2	48	0.31	transparent	21.989	44.865	0.7
65	10	0.3	24	0.38	transparent	21.779	44.333	0.6
63	10	0.3	48	0.48	transparent	21.771	44.286	1.3
59	10	0.4	48	0.29	transparent	21.637	44.032	0.8
				CAP Oxide				
39	6	0.3[c]	48	0.49	transparent	21.495	43.671	0.8
33	10	0.1[c]	24	0.08	slightly opaque			
61	10	0.2[c]	48	0.38	transparent	21.929	44.663	0.4
28	10	0.3[c]	24	0.22	transparent	21.772	44.365	1.2
35	10	0.3[c]	48	0.23	transparent	21.781	44.341	0.8
60	10	0.4[c]	48	0.22	transparent	21.571	43.678	0.9

[a] Zr/(Zr + Ti) = 0.70; Pb/(Zr + Ti) = 1.1—for all reactions. [b] Stronger peak. [c] Sum of TiO_2 and $ZrO_2 \cdot nH_2O$ concentrations.

amounts of $Zr(OC_3H_7)_4$ and Ti(*i*-$OC_3H_7)_4$ were added to 2-propanol (histological grade, Fisher Scientific) to obtain a solution with a total alkoxide concentration of 2.4 vol %. Subsequent hydrolysis of this solution at room temperature by a mixture of CO_2-free water and 2-propanol (with an alcohol-to-water volume ratio of 6.5) produced a coprecipitated gel. The hydrous oxide was centrifuged to remove alcohol, redispersed in deionized water and centrifuged two more times, and immediately used in the hydrothermal process. This precursor was characterized in a manner similar to that described for the SAP oxide.

Crystalline Amorphous Precursor (CAP). Titanium dioxide, TiO_2 (P25, Degussa, Akron, OH, 85 vol % anatase and 15 vol % rutile), and zirconium oxychloride, $ZrOCl_2 \cdot 8H_2O$ (98%, Aldrich), were used as received. Throughout the paper this precursor is referred to as a crystalline amorphous precursor oxide (the CAP oxide) since it consists of crystalline TiO_2 and amorphous hydrous zirconia oxide, $ZrO_2 \cdot nH_2O$, that forms when $ZrOCl_2 \cdot 8H_2O$ is added to a KOH aqueous solution at room temperature. To evaluate the characteristics of hydrous zirconia oxide $ZrO_2 \cdot nH_2O$, $ZrOCl_2 \cdot 8H_2O$ powder was added to a KOH aqueous solution at room temperature under vigorous stirring. The resulting powder was recovered by filtration, washed with water, dried, and analyzed for the water content, particle size, and surface area as described for the SAP oxide. Crystallite size was calculated from the specific surface area data, assuming the density of the amorphous $ZrO_2 \cdot nH_2O$ oxide as 3.25 g/cm^3.[26] The Degussa TiO_2 powder was examined with electron microscopy.

Single-Crystal Substrates. Epitaxial-grade single-crystal 5 × 5 mm^2 cubic $SrTiO_3$ (100) and pseudocubic $LaAlO_3$ (100) were used as substrates (Coating and Crystal Technology, Inc., Kittanning, PA). All substrates were polished on two sides. The lattice mismatch to the $PbZr_{0.7}Ti_{0.3}O_3$ (PZT) phase is 5.2% for $SrTiO_3$ and 8.4% for $LaAlO_3$. The growth experiments on $LaAlO_3$ substrates were conducted primarily to determine the composition of PZT films by EDS analysis. Prior to the hydrothermal process, substrate orientation was confirmed by X-ray diffraction analysis, and substrates were cleaned with trichloroethane, acetone, and 2-propanol, and dried at ≈70 °C.

3. Hydrothermal Synthesis. Hydrothermal syntheses of PZT thin films on single-crystal substrates were performed in Teflon-lined stainless bombs (110 mL, Parr Company, Moline, IL). Oxide precursor (either SAP, NAP, or CAP), lead acetate trihydrate, $Pb(OAc)_2 \cdot 3H_2O$ (certified A.C.S., Fisher Scientific), and potassium hydroxide (technical flakes, Fisher Scientific), which served as a pH-adjusting agent, were either dissolved or dispersed in water in a Teflon liner. The total amount of water used was ≈50 g. After the solution was thoroughly mixed, the stir bar was removed and either $SrTiO_3$ or $LaAlO_3$ substrate was placed at the bottom of the Teflon liner. Before closing, the Teflon liner was flushed with nitrogen. The autoclave was then placed in a box-type oven (Fisher) with a temperature control of ±1 K. All experiments were carried out at 150 °C. Highly alkaline KOH aqueous solutions (6, 8, 9, 10, and 12 *m*) were studied as a function of nutrient concentrations (0.1−0.4 *m*) and time (24, 48, and 60 h). A summary of reactions is presented in Table 1.

4. Thin Film and Powder Characterization. After a hydrothermal reaction was completed, the substrate was rinsed with water and dried with 2-propanol. Likewise, the powder that formed in the course of the hydrothermal reaction was rinsed with water and stored under ethanol. The latter was characterized using powder X-ray diffraction (XRD). The analyses were performed on a Siemens D-500 diffractometer (Siemens Analytical X-ray Instrument Inc., Madison, WI) using Ni-filtered Cu Kα radiation, in the 20−60° range with a 0.05° step size and 2-s count time. The chemical identity of the powder was determined by comparing the experimental XRD patterns to standards compiled by the Joint Committee on Powder Diffraction and Standards (JCPDS).

Dry substrates were characterized in terms of weight gain (accuracy ±0.5 mg) and transparency. The orientation of the film was confirmed by coupled θ−2θ scans in the 20−50° range with a 0.05° step and 2-s count time, using a Siemens D-500 diffractometer. The out-of-plane alignment between growth

(26) *Handbook of Chemistry and Physics*, 68th ed.; Weast, R. C., Astle, M. J., Beyer, W. H., Eds.; CRC Press: Boca Raton, FL, 1987−1988; p B-145.

Table 2. Water Content, Specific Surface Area, and Average Crystallite and Particle Sizes of Precursors Used in the Hydrothermal Syntheses of PZT

precursor type	water content (%)	specific surface area (m^2/g)	crystallite size (nm)	particle size (nm)
SAP	33	70−120	16−28	570
NAP	64	300	6	200
TiO_2	1	50[a]	21[a]	200[a]
$ZrO_2 \cdot nH_2O$	26	310	5	

[a] M. Holtman (Degussa Corporation), private communication.

plane normals of the film and the substrate was assessed by ω-rocking curves of the PZT (200) peak, also collected with a Siemens D-500 diffractometer. Full-width at half-maximum (FWHM) values were calculated with commercial software (Jade 3.1, MDI, Livermore, CA). The in-plane epitaxy was determined by X-ray pole figure analysis of PZT {310} peaks measured at $2\theta = 72.5°$ using a Phillips X'Pert Materials Research Diffractometer (MRD) system (Phillips, Mahwah, NJ) with Cu Kα radiation and incident and diffracted beam graded multilayer mirrors. The film microstructures of carbon-coated samples (films on $LaAlO_3$) and uncoated samples (films on $SrTiO_3$) were examined using FESEM, with an accelerating voltage of ≈5 keV. Semiquantitative analyses were carried out on a PGT (Princeton Gamma Tech, Princeton, NJ) EDS spectrometer, using an accelerating voltage of 20 keV.

Results

1. Precursor Characteristics. Table 2 contains data on some physical properties of precursors used in the hydrothermal syntheses of PZT thin films in this work. SAP, NAP, and $ZrO_2 \cdot nH_2O$ oxides were amorphous, as determined by X-ray diffraction analysis. The NAP precursor has a secondary particle diameter of ≈200- and 6-nm primary crystallite size based on FESEM and surface area measurements, respectively. An average diameter of 653 nm (number-weighted average) obtained with DLS indicates that the secondary particles were agglomerated or aggregated to some extent. For the CAP precursor, surface area measurements show that the primary crystallite size of the $ZrO_2 \cdot nH_2O$ is ≈5 nm. Extensive agglomeration/aggregation prevented accurate measurement of the secondary particle size or degree of agglomeration/aggregation with FESEM or DLS. The TiO_2 component of the CAP oxide had a primary crystallite size of ≈21 nm and a secondary particle diameter of ≈200 nm, as provided by the manufacturer. The latter was confirmed in our laboratory with FESEM. For the SAP oxide, a secondary particle diameter of ≈570 nm (number-weighted average) obtained by DLS is in agreement with FESEM observations. FESEM micrographs also confirmed that secondary particles had spherical morphology. These secondary particles were comprised of 16−28-nm primary crystallites, as estimated by surface area measurements. Since the SAP oxide used in this work was richer in Zr content than that of Choi et al.,[24] the secondary particle diameter of the SAP oxide is consistent with their findings. The composition of the SAP oxide was found by EDS standardless analysis to have a Zr:Ti ratio of 70:30, as expected. The compositional uniformity of Zr and Ti in the SAP oxide was examined by the method described previously for the NAP oxide.[22] The SAP oxide was calcined at 1100 °C for 24 h and analyzed by powder X-ray diffraction. The XRD analysis of the calcined sample suggested a $Zr_{0.7}Ti_{0.3}O_2$ solid solution rather than a mixture of separate ZrO_2 and TiO_2 phases. Although no JCPDS standard is available for a mixed $Zr_{0.7}Ti_{0.3}O_2$ oxide, the obtained XRD pattern exhibited a high degree of similarity to the XRD pattern of srilankite, $Zr_{0.5}Ti_{0.5}O_2$ (JCPDS Card No. 35-0584). Moreover, no peaks of known ZrO_2 and TiO_2 phases were detected.

2. Film Characteristics. Table 1 lists reaction conditions, substrate weight gains indicating the weights of the resulting PZT films, and the description of the obtained thin films prepared from the SAP oxide. Table 1 also contains similar results of selected reactions using the NAP oxide and CAP oxide that were carried out for the comparison.

Consistent with the thermodynamic predictions, all experimental conditions, represented by the points located in the area of the stability and yield diagram (Figure 1) with at least 93% yield, lead to the formation of a PZT thin film and PZT powder with rhombohedral symmetry, as indicated by the results of XRD analyses. Regardless of the oxide precursor used, the only experiments that yielded amorphous powder corresponded to a low precursor concentration (0.1 *m*), 10 *m* KOH, and a predicted PZT yield of 74%. On the other hand, even under these conditions, FESEM examination of the $SrTiO_3$ substrate surface for the SAP oxide revealed a deposit consisting of irregular particles up to 100 nm in size. Similar conditions for the other two types of precursor produced a film consisting of cube-shaped particles with the edge length of ≈1 μm. XRD patterns of these deposits were inconclusive in identifying the phase composition.

Preliminary growth experiments with 0.3 *m* SAP oxide concentration reveal that this precursor requires longer synthesis time than the other two precursors. Experiments carried out under the same conditions (KOH, 10 *m*; precursor, 0.3 *m*; temperature, 150 °C) did not produce a continuous film after 24 h using the SAP oxide (Figure 2a), in contrast to when either the NAP oxide (Figure 2b) or the CAP oxide (Figure 2c) was used. Only after a longer synthesis time of 48 h, a continuous film was observed when the SAP oxide was used. An even greater increase of the reaction time to 60 h did not increase the substrate weight gain significantly (cf. Table 1, reactions 41 and 56). This is an indication that at 150 °C the SAP oxide reacted almost completely to produce PZT powder and film after ≈48 h. Hence, the synthesis time for most experiments was set to 48 h.

The growth mechanism using SAP oxide resembled that reported by Chien et al.[9] As shown in Figure 2a, the epitaxial growth is initiated by the formation of {100} islands followed by their growth and coalescence.

A summary of substrate weight gains (Table 1) shows that after a hydrothermal process only a small fraction of the reactants transformed into PZT films. The average film thickness was estimated assuming a film density of 8 g/cm^3 and uniform coverage of both sides of the 5 × 5 mm^2 substrate. For example, weight gain of 0.35 mg corresponds to an average film thickness of 0.88 μm. On the basis of this assumption, the thickness of the films ranged from 2 to 0.2 μm. For all precursors employed, the weight deposited on the $SrTiO_3$ substrates diminished with an increase of KOH concentration in the hydrothermal solution. The dependence of film thickness on precursor concentration was difficult

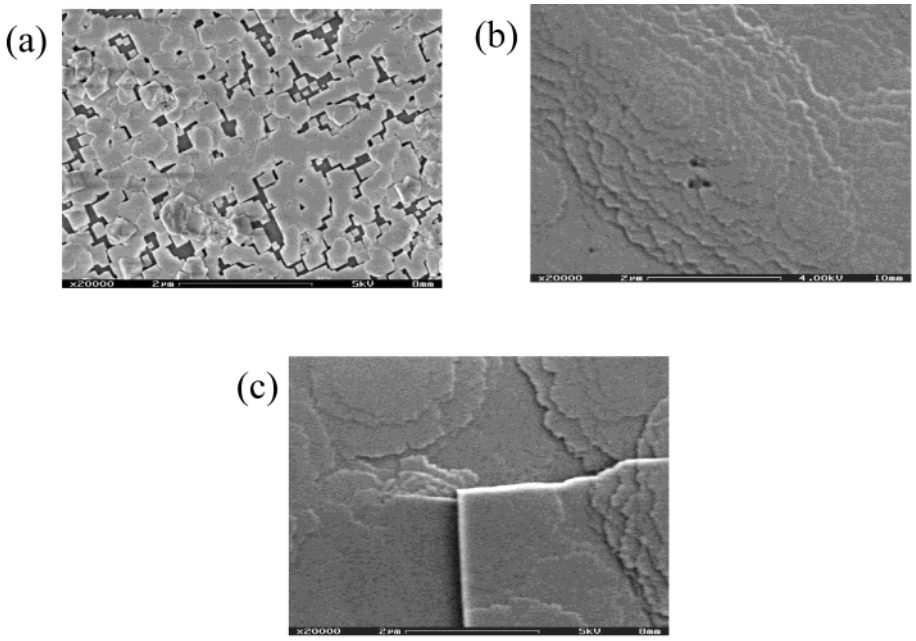

Figure 2. FESEM images of PZT films formed after 24 h at 150 °C from 10 *m* KOH solution with a precursor concentration of 0.3 *m*: (a) SAP oxide; (b) NAP oxide; (c) CAP oxide.

to assess because of film peel-off, which occurred at higher precursor concentrations (0.3 and 0.4 *m*). The films prepared from the SAP oxide were optically transparent when the KOH concentration was at least 9 *m*. Likewise, a high KOH concentration was necessary to produce transparent film using the NAP oxide (ref 21, Table 1 this work). However, the CAP oxide allowed the formation of a transparent PZT film already at a KOH concentration as low as 6 *m* (ref 9, Table 1 this work).

X-ray Diffraction and Phase Composition. The orientation and crystal quality of PZT thin films were determined by X-ray diffraction analysis. The 2θ values of PZT (100) and (200) peaks as well as the FWHM values of the PZT (200) peak, as determined from XRD patterns, are listed in Table 1. All films were regarded as epitaxial since only (100) and (200) peaks of PZT and $SrTiO_3$ were observed in the collected XRD data. The degree of alignment of a film with respect to the $SrTiO_3$ substrate was further investigated by collecting ω-rocking curves of the PZT (200) peak. The films obtained from the SAP oxide exhibited the FWHM values from several degrees to ≈1°. Raising the mineralizer concentration improved the out-of-plane alignment between growth plane normals of the film and the substrate, as can be inferred from the decreased FWHM value (cf. Table 1, reactions 40, 52, and 36).

X-ray pole figure analysis of the representative PZT film (0.4 *m* SAP oxide, 10 *m* KOH, 48 h, 150 °C) confirmed the in-plane alignment of the crystal axes of the film and $SrTiO_3$ substrate. Two sets of four peaks at $\psi \approx 18°$ and $\psi \approx 72$ °, evenly spaced in ϕ, were observed, without any extraneous film peaks, indicating a 4-fold symmetry and excellent in-plane alignment of the film and substrate lattice. The films grown from a solution containing either the NAP oxide or the CAP oxide and otherwise under similar conditions also exhibited a high degree of both in-plane alignment of the crystal axes of the film and substrate and alignment with respect to the $SrTiO_3$ substrate, as reported by Pinceloup et al.[21] and Chien et al.,[9] respectively.

XRD data summarized in Table 1 reveal that XRD patterns of PZT films, grown using the SAP oxide, are influenced by the KOH and precursor concentrations. An increase of the KOH concentration leads to the shift of PZT (100) and (200) peaks toward higher 2θ values (cf., Table 1, reactions 40, 52, 36, and 43). The same trend was observed for the XRD patterns of PZT films prepared from two other precursors (that is, the NAP oxide and the CAP oxide) as well as films grown on $LaAlO_3$ substrates using the SAP oxide. Moreover, the increase of the SAP oxide precursor concentration from 0.2 to 0.4 *m* causes the shift of PZT (100) and (200) peaks toward lower 2θ values (cf., Table 1, reactions 42, 36, and 41). This downward shift was also observed for PZT films prepared under similar experimental conditions from the other two precursors as well as films grown on $LaAlO_3$ substrates using the SAP oxide.

Standardless EDS analyses carried out for PZT films prepared at 6 and 10 *m* KOH (0.3 *m* SAP oxide, 48 h, 150 °C) revealed that in both samples the actual ratio of Zr to Ti was 78:22 and close to the targeted ratio of 70:30, which was within experimental error of the EDS method. The Pb-to-K ratio in the film prepared from the 10 *m* KOH solution was 91:9 while at 6 *m* KOH this ratio increased to 97:3. Standardless EDS analyses were also performed on PZT films prepared at 0.2, 0.3, and 0.4 m of the SAP oxide (10 *m* KOH, 48 h, 150 °C). The PZT film prepared at the lowest precursor concentration (0.2 *m*) has a Zr:Ti ratio of 62:38, within experimental error, whereas this ratio increases to 78:22 for the PZT film prepared at higher concentrations, that is, 0.3–0.4 *m*.

Film Microstructure. FESEM images of PZT thin films obtained from the SAP oxide are presented in Figures 3 and 4. Figure 3 shows KOH concentration effect and Figure 4 shows that of precursor concentration on PZT film microstructure.

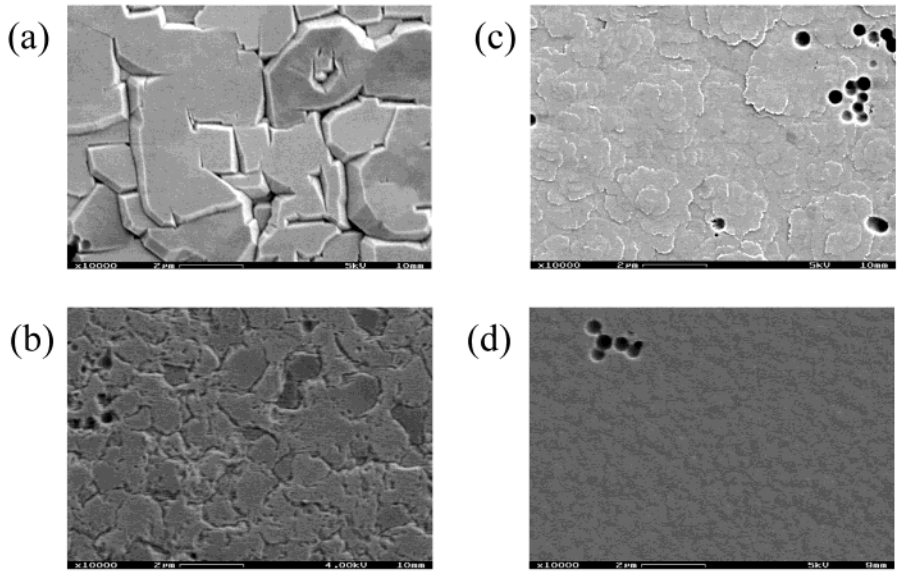

Figure 3. Changes in PZT film microstructure formed under increasing KOH concentration: (a) 6 *m* KOH; (b) 8 *m* KOH; (c) 10 *m* KOH; (d) 12 *m* KOH; (0.3 *m* SAP, 48 h, 150 °C).

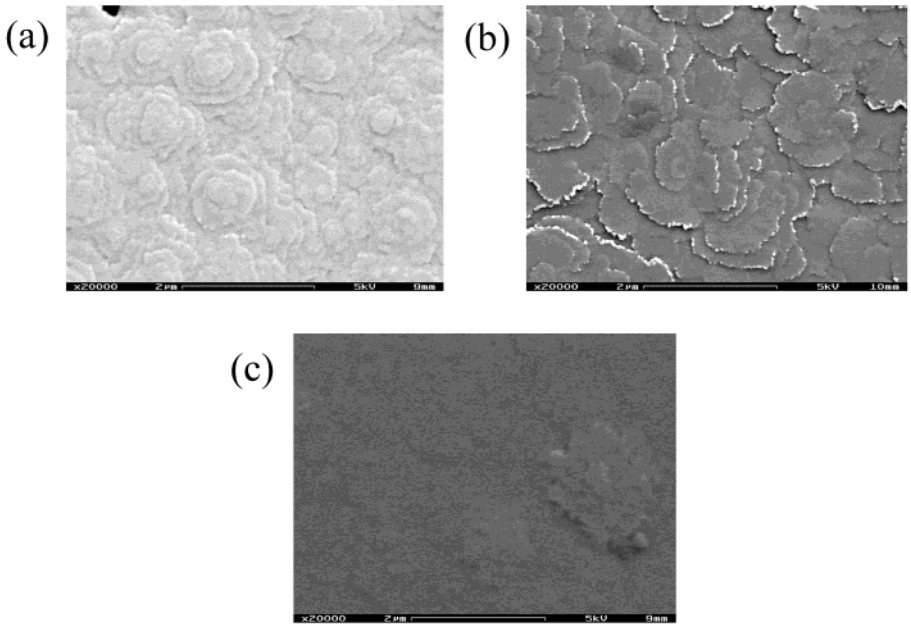

Figure 4. Changes in PZT film microstructure formed under increasing SAP oxide concentration: (a) 0.2 *m* SAP; (b) 0.3 *m* SAP; (c) 0.4 *m* SAP; (10 *m* KOH, 48 h, 150 °C).

As demonstrated in Figure 3, an increase in KOH concentration had a pronounced effect on the microstructure of the PZT films. A mosaic-like microstructure formed at lower mineralizer concentration (6 and 8 *m* KOH), which accounted for the observed lack of transparency of these films (Figures 3a and 3b, respectively). The surface of the transparent PZT film obtained at 10 *m* KOH was characterized by numerous circular overlapping patterns that are around 1−3 μm in size (Figure 3c), which suggested the presence of screw dislocations. A further increase of KOH concentration to 12 *m* resulted in a transparent, smooth film with a surface roughness <500 nm (Figure 3d). These changes in the microstructure with an increase of KOH concentration were accompanied, as already pointed out earlier by a decrease of both the FWHM value of the PZT (200) peak and substrate weight gain (Table 1). The spherical pores in Figure 3 seemed to be relics of the spherical morphology of the SAP precursor. The spherical particles probably deposited on the substrate and were consumed during the course of epitaxial crystallization, leaving behind spherical voids.

Examination of the microstructure of PZT films, formed at 6 and 10 *m* KOH, by using either the NAP oxide or the CAP oxide, revealed that films formed from the NAP oxide exhibited similar behavior to those formed using the SAP precursor. An increase in KOH concentration resulted in an improvement of film quality, as indicated by a change in the film microstructure from mosaic-like to smooth with circular overlapping patterns and by a decrease in FWHM value (Table 1). In contrast, KOH did not have a similar effect on films produced by using the CAP oxide. The film grown at 6 *m* was smooth and did not exhibit a mosaic-like structure. The film obtained at 10 *m* KOH was smooth with a circular overlapping pattern but features extensive

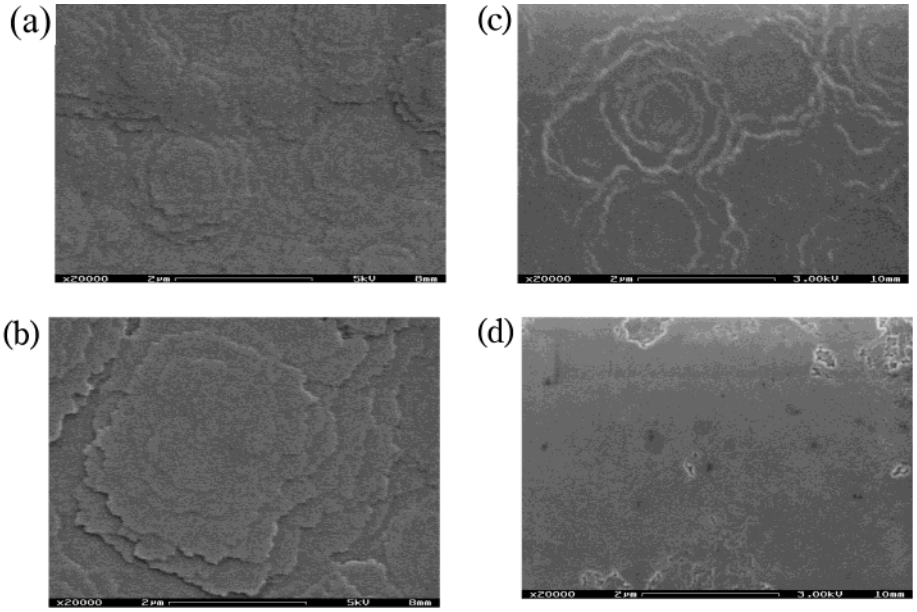

Figure 5. Changes in PZT film microstructure formed under increasing NAP and CAP oxide concentration: (a) 0.2 *m* NAP; (b) 0.4 *m* NAP; (c) 0.2 *m* CAP; (d) 0.4 *m* CAP; (10 *m* KOH, 48 h, 150 °C).

peel-off. Both films had excellent out-of-plane alignment, as indicated by fairly narrow FWHM values of the PZT (200) peak of ≈0.8° (Table 1).

The effect of precursor concentration on film microstructure was examined based on Figure 4. Figures 4a, 4b, and 4c show microstructures of films grown from the solution with SAP oxide concentration of 0.2, 0.3, and 0.4 *m*, respectively. For comparison, FESEM images of films grown under similar experimental conditions from the NAP oxide are shown in Figures 5a, 2b, and 5b, while Figures 5c, 2c, and 5d show FESEM images of films produced from the CAP oxide. A PZT film grown from 0.2 *m* solution of the SAP oxide produced a uniform coverage of the substrate with the microstructure characterized by concentric layers with a decreasing diameter (down to ≈500 nm) grown one on top of the other, as shown in Figure 4a. The other two precursors also produced uniform films with similar morphology (Figures 5a and 5c). An increase of precursor concentration to 0.3 *m*, regardless of precursor type, led to the partial coalescence of the concentric layers observed at the lower concentration and microstructures as shown in Figures 4b, 2b, and 2c. Although these three films exhibited similar microstructures, only the film obtained from the SAP oxide formed a uniform layer. The other two films exhibited peel-off in some regions of the film. The peel-off of a growing film from either a substrate or a film layer already deposited on the surface became even more pronounced with a further increase of the precursor concentration. For all precursors studied, films grown from the 0.4 *m* solution peeled off to some extent. On the other hand, PZT films grown at this precursor concentration and high KOH concentration (10 *m*) were very smooth with little porosity, especially those prepared by using either the SAP oxide or the CAP oxide (Figures 4c and 5d, respectively).

Discussion

Results of our study demonstrate that the quality, composition, and morphology of the epitaxial hydrothermal PZT films depend on the precursor choice, precursor concentration, and KOH mineralizer concentration. The effect of other processing variables, including reaction temperature and stirring, will be presented elsewhere.[27]

The markedly different reactivity of the SAP oxide as compared to that of the other two precursors studied in this work might be ascribed to its larger particle size and/or smaller specific surface area (Table 2). A similar dependence of reactivity on the size and/or nature of reacting species was reported by other authors.[28,29] For example, in the hydrothermal synthesis of phase-pure lead-based perovskite, nanosized crystalline titania (Degussa), the same as that used here, was reported to react faster than either micrometer-sized crystalline rutile or freshly precipitated alkoxy-derived amorphous hydrous titania.[28] On the other hand, in the hydrothermal synthesis of $BaTiO_3$ powder, amorphous hydrous titania particles (0.65 μm) dissolved more readily under hydrothermal conditions than smaller crystalline rutile particles (0.49 μm).[29] Also, the reactivity of the rutile is known to be lower than the reactivity of the anatase that constituted almost 85 vol % of the crystalline titanium dioxide used in this work.[22]

For all precursors, an increase of KOH concentration causes the shift of PZT (100) and (200) peaks toward higher 2θ values and a substrate weight gain decrease. In addition, for films prepared using either the SAP oxide or the NAP oxide, the FWHM value of the PZT (200) peak decreases and the film appearance changes from opaque to transparent, which is accompanied by a microstructure change from mosaic-like to smooth with a surface roughness <500 nm. PZT films synthesized using the CAP oxide are transparent for all KOH concentrations studied with fairly narrow FWHM's

(27) Suchanek, W. L.; Oledzka, M.; Mikulka-Bolen, K.; McCandlish, L. E.; Riman, R. E., manuscript in preparation.
(28) Gersten, B. L. Ph.D. Thesis, Rutgers, the State University of New Jersey, New Brunswick, May 1998, and references therein.
(29) Kumazawa, H.; Annen, S.; Sada, E. *J. Mater. Sci.* **1995**, *30*, 4740.

(<1°), indicative of high crystallinity and little if any porosity.

Kawano et al.[30] reported that a KOH concentration increase from 2 to 8 M decreased the FWHM value for hydrothermally grown polycrystalline lanthanum-doped PZT (PLZT) films on titanium substrates. An increase in the size of cube-shaped grains accounted for the decrease of the FWHM value of the PLZT (100) peak, which was attributed to enhanced reactant solubility at high KOH concentration.[30] The increase in grain size also suggested that PLZT nucleation rates were suppressed while growth rates were increased with increasing KOH molality. The work of Kawano et al. contrasted with the crystallization experiments presented here, where increased KOH concentrations from 6 to 10 *m* reduced the mass of PZT deposited on $SrTiO_3$ rather than increase it. A corresponding transition from mosaic to smooth film morphology was observed while they observed no transition. Our results suggest that increased KOH molality accelerates the nucleation rate but suppresses the growth rate. Experimental conditions might account for observed differences. In our work, the precursor suspension provided the titanium while Kawano et al. used a titanium metal substrate as a source of titanium. Moreover, changing the KOH concentration might change the reaction and/or crystallization mechanism. Gersten reported changes in activation energy from 101 to 47 kJ/mol when the KOH concentration increased from 2.5 to 7.8 *m* for the hydrothermal crystallization of lead titanate powder.[28]

The effect of KOH concentration on film properties suggests that when either SAP oxide or the NAP oxide is used, the PZT thin film forms most likely by a dissolution−precipitation mechanism.[12] Despite a distinct difference in reactivity, manifested in a longer synthesis time for the SAP oxide, higher KOH concentration seems to enhance the dissolution of both the SAP oxide and the NAP oxide. This leads to the increased nucleation rate and formation of smooth films. The CAP oxide did not exactly follow this behavior, as shown by the formation of a smooth transparent film at a KOH concentration as low as 6 *m*. That might be suggestive of a higher nucleation rate, originating from higher reactivity and/or better solubility of the CAP oxide at lower KOH concentration as compared to the solubility of the hydrous oxide mixed gels.[31]

The observed shift of PZT (100) and (200) peaks toward higher 2θ values (corresponding to a decrease of interplanar distances) could be related to the incorporation of potassium ions into the perovskite structure and/or lower zirconium content. From size considerations, K^+ ions most likely will enter the Pb^{2+} position (effective ionic radii of 1.78 and 1.63 Å, respectively: ref 32), creating vacancies in the oxygen position that subsequently shrink the cell size.[33,34] On the other hand, the phase diagrams for bulk PZT ceramics[35] and for PZT thin films[3] show a decrease in the unit cell parameter with a reduction in the Zr content in the rhombohedral part of the diagram. Thus, Zr deficiencies may be the source of this peak shift also. However, results of the EDS analyses performed on films processed in 6 and 10 *m* KOH solutions suggest that potassium ion incorporation is the cause. This finding is not surprising considering that alkali hydroxides and/or alkali halides, commonly employed as mineralizers, are often incorporated into the hydrothermally synthesized PZT powders.[36] Such incorporation has not been investigated as of yet for the hydrothermally synthesized PZT thin films. The observed competition of K^+ ions and Pb^{2+} ions for the "A" site, especially at higher KOH concentration, might be prevented by using a large excess of lead with respect to the stoichiometric composition (on the order of ≈25%). This idea was demonstrated by Ohba et al. when a 10 M KOH mineralizer concentration was used to make stoichiometric PZT powder that was free of significant K^+ incorporation.[31]

Regardless of the type of precursor used, an increase of precursor concentration leads to the shift of PZT (100) and (200) peaks toward lower 2θ values. On the basis of the results of the EDS analysis, the observed shift with an increase of a precursor concentration from 0.2 *m* to either 0.3 or 0.4 *m* could originate from the increase in the zirconium content and a slight decrease in the potassium content. The yield diagram in Figure 1 shows that experiments run at precursor concentrations of 0.3 and 0.4 *m* and a KOH concentration of 10 *m* should lead to the formation of the $PbZr_{0.70}Ti_{0.30}O_3$ phase with a high yield (i.e., 99.9%). In view of thermodynamic calculations and similar results of EDS analyses for films grown at these two higher precursor concentrations, it is difficult to rationalize the observed downward shift in 2θ values for (h00) peaks. More detailed analyses of these two films should be carried out to clarify the observed effect. For example, it has been observed for the PZT films, hydrothermally grown from the NAP oxide, that the local Zr-to-Ti ratio may vary from the nominal composition depending on the distance from the film/substrate interface, with layers closer to the interface being more Ti-rich.[21] Also, the *d*-spacing measured by XRD might be affected by strain in the film (e.g., epitaxial strain and thermal strain).[37]

The tendency of the film to peel off was more pronounced when reactant concentrations were set at high levels (e.g., 10 *m* KOH and 0.4 *m* precursor). General factors pertaining to adhesion of epitaxial films have been discussed in detail elsewhere (e.g., refs 38 and 39). Interfacial stress is an important factor. The lattice mismatch between $PbZr_{0.7}Ti_{0.3}O_3$ and $SrTiO_3$ (≈5.2%) could be sufficient to induce considerable internal stress in the film. XRD peak shifts show that increasing precursor concentration for all precursors increased the interplanar distances, further worsening

(30) Kawano, T.; Nagao, K.; Hashimoto, K. *Integr. Ferroelectr.* **1996**, *12*, 263.
(31) Ohba, Y.; Rikitoku, T.; Tsurumi, T.; Daimon, M. *J. Jpn. Ceram. Soc.* **1996**, *104*, 6.
(32) Shannon, R. D. *Acta Crystallogr.* **1976**, *A32*, 751.
(33) Jaffe, B.; Cook, W. R., Jr.; Jaffe, H. *Piezoelectric Ceramics*; Academic Press: London and New York, 1971; p 159.
(34) Tan, Q.; Xu, Z.; Li, J.-F.; Viehland, D. *J. Appl. Phys.* **1996**, *80*, 5866.
(35) Fushimi, S.; Ikeda, T. *J. Am. Ceram. Soc.* **1967**, *50*, 129.
(36) Beal, K. In *Advances in Ceramics*; Messing, G. L., Mazdiyashi, K. S., McCauley, J. W., Haber, R. A., Eds.; American Ceramic Society: Westerville, OH, 1987; Vol. 21 (*Ceramic Powder Science*), p 33.
(37) Segmüller, A.; Murakami, M. in *Thin Films for Free Atoms and Particles*; Klabunde, K. J., Ed.; Academic Press: Orlando, 1985; p 325.
(38) Kuech, T. F. In *Electronic Materials Chemistry*; Pogge, H. B., Ed.; Marcel Dekker: New York, 1996; p 103.
(39) Chernov, A. A. *Modern Crystallography III*; Springer-Verlag: Berlin, 1984; pp 85−103, and references therein.

the lattice mismatch, which might explain why peel-off was observed for all precursor systems at increasing precursor concentrations. However, lattice mismatch might not be the controlling factor. In the case of films grown from the CAP precursor, an increase in KOH concentration assisted in film peel-off. XRD analyses show a decrease in the interplanar distances with increasing KOH concentration, which means that the film lattice parameters and lattice mismatch are decreased due to potassium incorporation. Thus, increasing KOH concentration should decrease lattice stress to reduce peel-off instead of worsening the situation, as we observed. Hence, it is possible that the as-crystallized films exhibit peel-off due to other factors. Since hydrothermal reactions reported here were conducted in unstirred reactors, nonuniformities in the reactor may have led to compositional/physical heterogeneities in the film and/or at the film/substrate interface that caused peel-off but were not detected during film characterization. The hypothesis that peel-off is not dependent on lattice mismatch between the film and substrate is supported by the work of Kawano et al., who also observed peel-off as the KOH concentration was increased. Since their films were polycrystalline, film growth and peel-off would not be expected to be dependent on lattice strain (lattice mismatch) since the metal substrate offers many types of nucleation sites for growth of the grains in the film. Thus, the cause of peel-off for films prepared by Kawano et al. may be related to similar causes.

Conclusions

We have demonstrated that the amorphous Zr−Ti hydrous oxide composed of submicrometer spheres (the SAP oxide) can be employed as a precursor in the hydrothermal growth of $PbZr_{0.7}Ti_{0.3}O_3$ heteroepitaxial thin films. The lower reactivity of the SAP oxide was attributed to a larger particle size and/or smaller specific surface area as compared to those characteristics of two other precursors studied in this work. At a temperature of 150 °C, the SAP oxide produced the best film in terms of crystallinity and morphology after a 48-h-long reaction where the precursor concentration was either 0.3 or 0.4 *m* and KOH concentration was 10 *m*. For all precursors investigated, increased KOH and precursor concentration resulted in a faster nucleation rate that had a significant effect on film quality, morphology, and composition. The observed effect of KOH concentration on the film properties suggests that PZT thin film formation is most likely controlled by a dissolution−precipitation mechanism when either the SAP, CAP, or NAP oxide is used. Precursor choice determines the thin film growth conditions for making optically transparent films. The SAP and NAP oxides required a KOH concentration of at least 9 *m* to produce a smooth transparent film, whereas the CAP oxide allowed the formation of a transparent PZT at a KOH concentration of 6 *m*.

Acknowledgment. The authors would like to thank T. Hao for help in DLS particle size measurement, I. Pozsgai and Z. Kalman for helpful information and discussions, E. Gulliver for the EDS measurements, and A. T. Chien and B. Gersten for sharing copies of their theses. Financial support of ONR and DARPA is gratefully acknowledged.

CM020063B